Chaos, Solitons and Fractals 132 (2020) 109606

Contents lists available at ScienceDirect

Chaos, Solitons and Fractals

Nonlinear Science, and Nonequilibrium and Complex Phenomena

journal homepage: www.elsevier.com/locate/chaos

Frontiers

Analysis of multistability, hidden chaos and transient chaos in brushless DC motor

Philippe Faradja [a], Guoyuan Qi [b,*]

[a] School of Mechanical Engineering, Tiangong University, Tianjin 300384, PR China
[b] Tianjin Key Laboratory of Advanced Technology of Electrical Engineering and Energy, Tiangong University, Tianjin 300384, PR China

ARTICLE INFO

Article history:
Received 21 August 2019
Revised 21 December 2019
Accepted 3 January 2020
Available online 9 January 2020

Keywords:
BLDCM
PMSM
Hidden chaos
Transient chaos
Multistability
Homotopy

ABSTRACT

The dynamics of brushless DC motor (BLDCM), a type of permanent magnet synchronous motor (PMSM) is investigated. The dynamical model of the BLDCM is compared to a mostly used model of PMSM. The BLDCM transition to chaos is briefly investigated both on the local level through local bifurcations and global level through manifold and invariant sets. All the transition parameter values are given. Apart from transition, multistability of the BLDCM is observed and assessed with stability basin. For some parameter values all dynamic modes (stable fixed point, limit cycle, chaotic attractor) coexist. For other parameter values multistability concerns different stable equilibria. Also, hidden chaos which is of non-Shilnikov type is examined and reported in BLDCM with the method of homotopy. Hidden chaos is defined from the basin of attraction. Transient features of the hidden chaotic set are studied. Finally, transient time of hidden chaos improves with two methods: critical velocity (acceleration) surfaces and Broyden-Fletcher-Goldfarb-Shanno (BFGS) algorithm.

1. Introduction

Since the seminal work of Lorenz [1] in the study of weather predictions, research in chaos theory has taken various directions. The discovery and analysis of other chaotic systems [2–5] and hyperchaotic systems [6–7] have followed.

Different types of studies were conducted on these systems. Most of these chaotic systems were numerical, and therefore the interpretation of different dynamical behaviors was more conceptual than physical.

Chaos was also investigated in real physical systems [8]. In mechanical systems like double pendulum [9] or triple pendulum [10], chaos was observed theoretically and practically. In electromechanical systems such as the beam coupled with an oscillator [11], electromechanical transducer [12] or brushless DC motor (BLDCM) [13], chaos has been investigated.

BLDCM has been investigated for its advantages such as small size, high efficiency, high speed range and have been utilized in the automotive industry (electrical vehicles), the aerospace industry, and medical instrumentation [14–15].

In all these classical chaotic systems, whether numerical or physical systems, self-excited chaos was mostly investigated. Self-excited chaotic attractors are excited from unstable equilibria. Less than a decade ago, however, a new class of attractors were observed in Chua's circuit [16–18] and later in Rabinovich system, phase-locked loop, coupled Chua circuits [19], Lorenz-like systems [20]. These attractors are excited either without equilibrium or from stable equilibria.

The traditional Lorenz system was revisited and sufficient attention for hidden chaos was recently drawn. Munmuangsaen and Srisuchinwong [21] have shown with extensive computer search that classical Lorenz system possesses hidden chaotic attractor. Yuan *et al.* [22], also, studied the existence of hidden chaos in the traditional Lorenz system.

The interest in hidden chaos has increased as hidden chaos has become a new and promising research direction. For example, hidden hyperchaos has also been reported [23]. Although based on the dynamo, the system is still mathematical as two artificial states are added. And with hidden chaos, multistability becomes a specific feature of concern. Bridges have collapsed [24] and drilling rigs with induction motors [25] have failed due to uncontrolled multistability. Maybe the worst disaster came with 1992 YF-22 Boeing crash caused by the sudden shift to an undesirable attractor [26]. Coexistence of attractors have been found in hidden chaotic systems such as variable-boostable systems which possess no equilibrium and have been implemented electronically [27–29].

In this paper, hidden chaos, this new trend in chaos theory is investigated on BLDCM while physical meaning of parameters

* Corresponding author.
E-mail address: qiguoyuan@tjpu.edu.cn (G. Qi).

https://doi.org/10.1016/j.chaos.2020.109606
0960-0779/

is maintained. Although hidden chaos has been reported in permanent magnet synchronous motors (PMSM) recently [30], we make some comments on that paper while objecting to some results therein. The existence of extra equilibria influences the dynamics of a system to a large extent. In this way, multistability and coexistence of attractors of the BLDCM are investigated. Local bifurcation and global bifurcation (especially homoclinic manifold and transition from global stability to chaos) are analyzed. Most importantly, hidden chaos is reported in BLDCM. We extend previous work [31]. Although recent methods to localize hidden chaos include perpetual points (PP) [32–33], regular points [34], critical surfaces [35], the suitable method for BLDCM is homotopy [36]. And while in most recent studies on hidden chaos [21,22,30] transient behavior is just observed, our contribution also includes the description of transient properties and improvement of transient time of the BLDCM. To this end, critical surfaces and optimization method like Broyden-Fletcher-Goldfarb-Shanno (BFGS) [37] which have not been used in the study of transient properties are proposed.

The rest of paper is organized as follows. In Section 2 the model of BLDCM is compared to another model of PMSM and the choice of the model is justified. The transition of the BLDCM to chaos is described both locally and globally in Section 3. In Section 4, first multistability of BLDCM is analyzed. Then, hidden chaos is highlighted and the transient properties of BLDCM are studied. Finally, Section 5 concludes this paper.

2. BLDCM and PMSM models and real scenario

The non-salient-pole BLDCM model in the d-q rotating frame obtained after a Park transformation comprises differential equations for three state variables [13]:

$$\begin{aligned}\frac{di_q}{dt} &= (-Ri_q - nL\omega i_d - nk_t\omega + v_q)/L,\\ \frac{di_d}{dt} &= (-Ri_d + nL\omega i_q + v_d)/L,\\ \frac{d\omega}{dt} &= (nk_t i_q - b\omega + T_L)/J,\end{aligned} \tag{1}$$

where i_q the quadrature-axis current, i_d the direct-axis current, ω rotor velocity; t is the elapsed time; for the parameters, R is the winding resistance matrix with $L = \frac{3}{2}L_a$, L_a the self-inductance of the winding, n the number of permanent-magnet pole pairs, $k_t = \sqrt{3/2}k_e$, k_e the coefficient of motor torque, J the moment of inertia, b the damping coefficient; for the input variables, v_q and v_d are the voltages across the quadrature axis and direct axis, respectively, and T_L the external torque. This model describes a smooth air-gap machine where the variation of reluctance in the air gap L_g is zero.

Singh *et al.* [30] have described the possibility of existence of hidden attractor in PMSM. The model follows [38]:

$$\begin{aligned}\frac{di_q}{dt} &= (-Ri_q - nL\omega i_d - \psi_r\omega + v_q)/L,\\ \frac{di_d}{dt} &= (-Ri_d + L\omega i_q + v_d)/L,\\ \frac{d\omega}{dt} &= (n\psi_r i_q - b\omega - T_L)/J.\end{aligned} \tag{2}$$

The following transformation is made: $\gamma = -\frac{\psi_r}{kL_q}$, $\sigma = \frac{b\tau}{J}$, $\tilde{v}_d = \frac{1}{Rk}v_d$, $\tilde{v}_q = \frac{1}{Rk}v_q$, $\tilde{T}_L = \frac{\tau^2}{J}T_L$, $\tau = \frac{L_q}{R}$, $k = \frac{b}{n\tau\psi_r}$, $L_d = L_q = L$, $i_q = ky$, $i_d = kx$, $\omega = \frac{z}{\tau}$.

When $\tilde{v}_d = 0$, $\tilde{v}_q = 0$ and $\tilde{T}_L = 2\sin(\pi cy)$, Eq. (2) is transformed into the new model [30]:

$$\begin{aligned}\frac{dx}{dt} &= -x + yz,\\ \frac{dy}{dt} &= -y - xz + \gamma z,\\ \frac{dz}{dt} &= \sigma(y - z) - 2\sin(\pi cy).\end{aligned} \tag{3}$$

Some problems regarding the work in [30] are listed below.

2.1. Non-dimensionalization problem

The PMSMS model [Eq. (2)] is different from Hemati [13]'s BLDCM model [Eq. (1)]. Both models become similar under only one condition, when the number of pole pairs is one, i.e., $n = 1$. When the physical meaning of parameters of PMSM is kept, it is physically impossible to have chaos from the chosen parameters [30,38]. In order to have a positive γ as in the illustration of chaos, some parameters like ψ_r, L_q, n, L, R should be negative. This violates the real condition.

2.2. Problem of condition of stable equilibrium

According to Singh *et al.* [30], there is only one equilibrium, namely $S_0 = [0, 0, 0]^{\mathrm{T}}$. When $\sigma = 5.46$, $\gamma = 14.5$ and $c > 0.9$, this equilibrium is sink node. In fact, we obtain that all eigenvalues of the origin equilibrium are negative when $c > \frac{\sigma(\gamma-1)}{2\pi\gamma}$.

2.3. Problem of number of equilibrium points

Given $\sigma = 5.46$, $\gamma = 14.5$ and $c = 0.809466400974780$, the surprising fact is that the PMSM possesses other equilibria. Since we cannot not find these equilibria analytically we refer to the numerical methods. By applying unconstraint multi-objective optimization techniques, other equilibria are found. We briefly expose those equilibria and their stability condition for $c = 3.975$, the case described in the paper. The equilibria and their eigenvalues are highlighted in Table 1.

Among these five equilibria, only one equilibrium is focus-node sink. All the remaining four equilibria are of saddle type: two saddle focus and two saddle nodes. The effects of the equilibria on the generation of the chaos should be specified.

In the current paper the physical meaning of the BLDCM model's states and parameters is kept. The behavior has been analyzed and important features have been found by bifurcation [39].

When $v_q = 0$, $T_L = 0$, the BLDCM of Eq. (2) possesses three equilibria as

$$S_0 = \left[0, \frac{v_d}{R}, 0\right]^{\mathrm{T}} \text{ and } S_{1,2} = \left[\pm\frac{1}{n^2k_tL}\sqrt{\Delta}, -\frac{n^2{k_t}^2 + Rb}{n^2k_tL}, \pm\frac{1}{nbL}\sqrt{\Delta}\right]^{\mathrm{T}}$$

Table 1
Equilibria and eigenvalues of PMSM described by Eq. (3).

Equilibrium	Eigenvalue
$\begin{bmatrix}0.002960450076482\\ \pm0.207166024983329\\ \pm0.014290229689302\end{bmatrix}$	-0.999793435104483 -23.027584015877803 16.567377450982296
$\begin{bmatrix}0\\0\\0\end{bmatrix}$	$-3.23 + j16.673457744048275$ $-3.23 - j16.673457744048275$ -1.00
$\begin{bmatrix}13.460075522153391\\ \pm3.741318233785868\\ \pm3.597682603566530\end{bmatrix}$	$1.901238469646910 + j5.873946348053686$ $1.901238469646910 - j5.873946348053686$ -11.262476939293814

where $\Delta = -(bn^2Lk_tv_d + Rbn^2{k_t}^2 + R^2b^2)$. Therefore we have one equilibrium on the symmetric axis (S_0) and two symmetric equilibria ($S_{1,2}$).

The scenario of multistability in the BLDCM is discussed in Section 4 for a certain range of parameters. The following values of parameters given by Hemati [13] are used: $k_t = 0.031$Nm/A, $n = 4$, $L = 14.25 \times 10^{-3}$H, $R = 0.9\ \Omega$, $b = 0.0162$ Nm/rad/s, $J = 4.7 \times 10^{-5}$Kgm^2, $v_q = 0$V, $T_L = 0$N.

3. Transition to chaos

In the study of dynamical systems, the transition to chaos has been studied. The transition can consider local features (local bifurcation) or global features (global bifurcation).

On the local level, different bifurcations have been studied. For example, pitchfork bifurcation exists when the number of equilibria change from three to one [39]. When there is one equilibrium, it is not only stable but also globally stable.

Theorem 1. *If $v_d > v_{dc}$ with $v_{dc} = -\frac{bR^2+k_t^2n^2R}{k_tLn^2}$, the BLDCM system's equilibrium is globally asymptotically stable.*

Proof: Set Lyapunov function

$$E = \frac{1}{2}\left(p_1 i_q^2 + p_2\left(i_d - \frac{v_d}{R}\right)^2 + p_3\omega^2\right), \tag{4}$$

where $p_1, p_2, p_3 > 0$. When $\|i_q, i_d, \omega\| \to \infty$, the Lyapunov function holds $E \to \infty$. And

$$\dot{E} = -\frac{Rp_1 i_q^2}{L} - \frac{Rp_2}{L}\left(i_d - \frac{v_d}{R}\right)^2 - \frac{bp_3\omega^2}{J} - np_1 i_q i_d\omega + np_2 i_q i_d\omega + \frac{nk_t p_3 i_q\omega}{J} - \frac{nk_t p_1 i_q\omega}{L} - \frac{nv_d p_2 i_q\omega}{L}. \tag{5}$$

Setting $p_1 = p_2$, then we have

$$\dot{E} = -\frac{Rp_1 i_q^2}{L} - \frac{Rp_1}{L}\left(i_d - \frac{v_d}{R}\right)^2 - \frac{bp_3\omega^2}{J} + \frac{nk_t p_3 i_q\omega}{J} - \frac{nk_t p_1 i_q\omega}{L} - \frac{nv_d p_1 i_q\omega}{L}. \tag{6}$$

Setting $F = \frac{L}{Rp_1}\left(\frac{nk_t p_3}{J} - \frac{nk_t p_1}{L} - \frac{nv_d p_1}{L}\right)$ with $p_1 \neq 0$.

$\dot{E} = -\frac{Rp_1 i_q^2}{L} - \frac{Rp_1}{L}(i_d - \frac{v_d}{R})^2 - \frac{bp_3\omega^2}{J} + \frac{FRp_1 i_q\omega}{L}$, so that

$$\dot{E} = -\frac{Rp_1}{L}\left(i_q - \frac{F\omega}{2}\right)^2 - \frac{Rp_1}{L}\left(i_d - \frac{v_d}{R}\right)^2 - \frac{bp_3}{J}\left(1 - \frac{JRp_1F^2}{4Lbp_3}\right)\omega^2. \tag{7}$$

$\dot{E} < 0$ when $(1 - \frac{JRp_1F^2}{4Lbp_3}) \geq 0$. This condition implies that p_3 is positive real coefficient only when $p_3 \in [p_{31}, p_{32}]$ and $v_d \geq -\frac{bR^2+k_t^2n^2R}{k_tLn^2}$ with $b, R, n, k_t > 0$.

As the Lyapunov function has been obtained such that $E > 0, E(S_0) = 0, \dot{E} < 0$, BLDCM's equilibrium is globally asymptotically stable in the range $v_d > v_{dc}$; the proof is complete.

There is also Hopf bifurcation which is an important transition at v_{dH}. The Shilnikov inequality $|\frac{\eta}{\gamma}| < 1$ holds with $\gamma < 0; \eta > 0$; $\varpi \neq 0$ when $v_d < v_{dH}$ as the symmetric equilibria have one real eigenvalue γ and two imaginary eigenvalues $\eta \pm j\varpi$. Therefore Shilnikov chaos [40–41] is present in BLDCM.

When $v_d = v_{dH}$, there is a coexistence of a periodic attractor and a chaotic attractor. The period attractor (limit cycle) can be localized locally around the symmetric equilibria.

Once, we obtained that $v_{dH} = \frac{-2J^2k_t^2R^2n^2 + Jk_t^2LRbn^2 + 4JLR^2b^2 + L^2Rb^3}{2J^2k_tLRn^2 - bJk_tL^2n^2}$ is the Hopf bifurcation voltage [39]. Table 2 gives all the parameter critical values when $k_t = 0.031$Nm/A, $n = 4$, $L = 14.25 \times 10^{-3}$H, $R = 0.9\ \Omega$, $b = 0.0162$ Nm/rad/s, $J = 4.7 \times 10^{-5}$Kgm^2, $v_q = 0$V, $T_L = 0$N.

In Table 2, S denotes saddle, UF unstable focus, SF stable focus, SF2 saddle focus with index 2 and SN stable node. In order to better illustrate the values, the following axis is given.

For a certain range $v_{dH} \leq v_d < v_{dcrit2}$ a type of chaotic attractor exists. This chaos is not of a Shilnikov type.

As observed [41], the symmetric equilibria are responsible for generating chaos. This observation is crucial for this study.

Regarding global manifold, we consider the case of the stable global manifold on the BLDCM first. When,$i_q = 0, \omega = 0$ from Eq. (1) then

$$\frac{di_d}{dt} = (-Ri_d + v_d)/L \text{ so that } i_d = \frac{v_d}{R} - \frac{v_d}{R}e^{-\frac{Rt}{L}} + i_d(0)e^{-\frac{Rt}{L}}.$$

When $t \to \infty$, $i_d = \frac{v_d}{R}$.

Trajectories starting from the initial conditions in this invariant set will remain in this set and this confirms the idea of manifold. The manifold is stable as the equilibrium will be reached in forward time. Thus the i_d-axis is always a part of the stable manifold for the equilibrium on the symmetric axis, the BLDCM model being symmetric [31].

On the global level, the homoclinic orbit and different global manifolds offer interesting features. The homoclinic bifurcation illustrates the qualitative change of properties on the global scale. When $v_d = v_{dHom}$ with $v_{dHom} = -15.453701864361906$V [Table 2, Fig. 1],

BLDCM undergoes the homoclinic bifurcation as illustrated in Fig. 2.

When $v_d > v_{dc}$, there is only one invariant set with one stable equilibrium as illustrated in Fig. 3(a).

When $v_{dHom} < v_d < v_{dc}$, there are three invariants sets: two invariant sets with one stable equilibrium each [Fig 3(b)] and one stable manifold (not plotted).

When $v_{dcrit1} < v_d < v_{dHom}$, there are three invariant sets: two invariant sets with the two stable equilibria [Fig. 3(c)] and one stable manifold (not plotted).

When $v_{dcrit2} < v_d < v_{dcrit1}$ there are four invariant sets: hidden chaotic set and two invariant stable sets (one for each stable equilibrium) [Fig. 3(d)]. The fourth set involves stable manifold of the origin (not plotted). Therefore, the basin of attraction is divided into four regions.

Table 2
Critical parameter values for evolution of dynamics.

$v_d < v_{dH}$	v_{dH}	v_{dcrit2}	v_{dcrit1}	v_{dHom}	v_{dc}	$v_d > v_{dc}$
1S, 2 SF2	1 S, 2UF	1 S, 2SF	1 S, 2 SF	1 S, 2 SF	1 SN	1 SN
< -29.67V	-29.67V	-28.62V	-28.53V	-15.4537V	-3.184V	> -3.184V

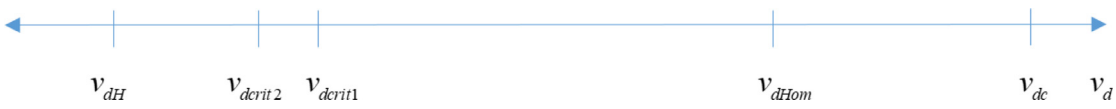

Fig. 1. Critical values of the bifurcation parameter for evolution of dynamics.

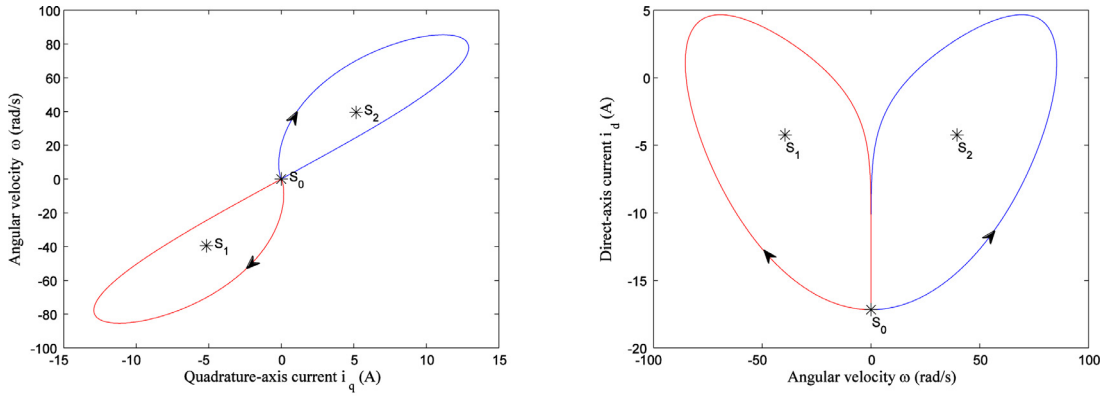

(a) $i_q - \omega$ plane (b) $\omega - i_d$ plane

Fig. 2. Projections of the homoclinic orbit.

When $v_{dH} < v_d < v_{dcrit2}$, the first three invariant sets fusion into a non-Shilnikov chaotic set [Fig. 3(e)]. The second set consists of stable manifold of the origin (not plotted).

With $v_d < v_{dH}$, the non-Shilnikov chaos turns into the self-excited Shilnikov chaos [Fig. 3(f)]. The second invariant set is the stable manifold of the saddle equilibrium. In Fig. 3(b–f), the trajectories in blue and red stem from initial conditions on the unstable manifold of the saddle equilibrium S_0 while the trajectories in green start from $[2, 2, 2]^{\mathrm{T}}$, which also used in Fig. 3(a).

Remark 1. Hidden chaos is mainly non-Shilnikov. Not every non-Shilnikov chaos is hidden.

In the next section, multistability, hidden chaos and transient behavior of this chaos are described.

4. Multistability, hidden chaos and transient properties

4.1. Multistability

The BLDCM demonstrates the feature of multistability. While local stability has been used to highlight the concept of multistability, limitations should be highlighted. Small disturbance convergence rate and linear stability are unreliable proxies of how stable a state is against non-small disturbances [42]. Basin stability is therefore preferred as it reveals features of global stability. Because of global features, basin stability addresses stability on all stable equilibria. The estimation of the basin stability is achieved as follows; N initial conditions are drawn randomly in a certain region and the system equations are integrated. The number of cases when stable equilibria are reached is counted as M and the ratio M/N is the stability basin estimate of those stable equilibria. For BLDCM, we define two regions:

$$I_{s_1} = \{(i_q, i_d, \omega)| -2.301 < i_q < 17.698, -2.301 < i_d < 17.698, 48.927 < \omega < 68.927\}, \text{ and}$$

$$I_{s_2} = \{(i_q, i_d, \omega)| -2 < i_q < 2, -2 < i_d < 2, -2 < \omega < 2\}.$$

In Fig. 4(a) the basin stability of BLDCM is defined around the symmetric equilibria in the I_{s_1} region while in Fig. 4(b) the basin stability in I_{s_2} is given.

When the basin stability is close to zero, BLDCM has a lower probability of converging to the stable nodes. When the stability is close to one, BLDCM has a higher probability to converge to stable nodes. In Fig. 4(a), where chaos and limit cycles coexist in the region I_{s_1}, basin stability is closer to zero around v_{dH} than in Fig. 4(b) where the stable manifold and chaotic region coexist. However, around v_{dcrit1} and v_{dcrit2}, the basin stability of I_{s_2} is closer to zero [Fig. 4(b)] than that of I_{s_1} [Fig. 4(a)]. For the rest of the range, basin stability is the same for both regions I_{s_1} and I_{s_2}.

The uncertainty of the final state is the major concern for the BLDCM, especially as the applications of the BLDCM vary according to the utility. Useful chaos for mixing, compacting and grinding will mainly focus on irregular oscillations that fulfil all the conditions of chaos. When chaos is detrimental, control and synchronization are needed. Yet multistability combines chaotic dynamics and non-chaotic dynamics.

As mentioned previously, for example, when $v_d = v_{dH}$, there is a coexistence of two periodic attractors (stable limit cycles) as illustrated in Fig. 5(a)-(b) when initial conditions $[\pm 7.6985, -4.2383, \pm 58.9271]^{\mathrm{T}}$ are around symmetric equilibria and a chaotic attractor in Fig. 5(d) with $[0.1, 0.1, 0.1]^{\mathrm{T}}$ as initial conditions.

Actually, there exists also a stable focus node when initial conditions are drawn from the stable manifold of the saddle equilibrium as in Fig. 5(c) with initial conditions at $[0, -10, 0]^{\mathrm{T}}$. This means that the final state can be of the three possibilities.

This case is even more interesting as it outlines the coexistence of three important dynamic behaviors: stable fixed points, limit cycle and chaos. These dynamic behaviors coexist for the same parameters subjecting only to the initial conditions change. Therefore, multistability concerns different dynamic behaviors. The physical meaning of initial conditions is important. For example, when the motor starts running with a negative angular velocity, the motor is rotating in clockwise direction, opposite with respect to the positive direction.

The main issue here involves the choice of desired equilibrium from specific initial conditions. In particular, the question becomes the following; which initial conditions lead to which equilibrium?

4.2. Hidden chaos

A crucial question needs an answer, which equilibrium produces chaos? According to Singh *et al.* [30], with the stable trivial equilibrium, hidden chaos is produced. But the generation of chaos by nontrivial equilibria is obvious with our system. The nontrivial (symmetric) equilibria are stable foci in the range of the study.

We recall that when $v_{dcrit2} < v_d < v_{dcrit1}$, there are four invariant sets: hidden chaotic set and two invariant stable sets (one for each stable equilibrium). This hidden chaos is defined as its basin of attraction does not intersect with the small vicinities of the saddle equilibrium. Hidden chaos in BLDCM follows more the patterns of a transient chaotic set than that of an attracting chaotic set (attractor) [43].

In this regard, the BLDCM demonstrates hidden transient chaotic set. The basin of the saddle equilibrium S_0 is viewed in

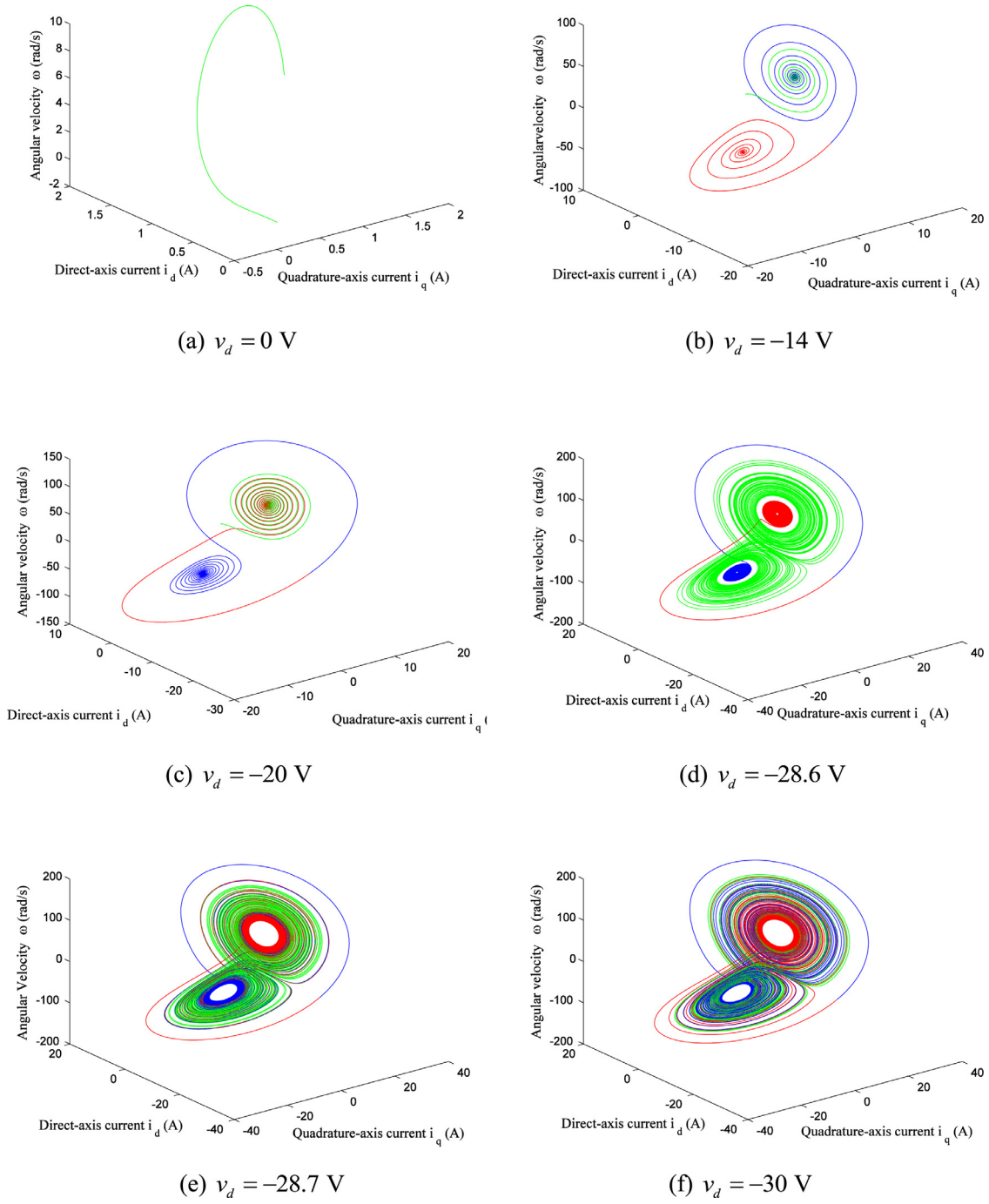

Fig. 3. From stability to self-excited chaos: attractors at different parameter values. (For interpretation of the references to color in the text, the reader is referred to the web version of this article.)

Fig. 6. The considered section is $i_d = \frac{v_d}{R}$, on which the equilibrium S_0 is located. Particularly, we choose $v_d = -28.6$V.

From Fig. 6, the chaos region of the basin is in green. The regions in blue and red belong respectively to the space of stability to the symmetric equilibria S_1 and S_2. Trajectories with initial conditions in the blue (red) stable region converge to the equilibrium $S_1(S_2)$. Clearly, the basin of attraction of chaotic set in green color does not intersect with the saddle equilibrium S_0 and this confirms the existence of hidden chaotic set.

In fact, Fig 6 describes the basin of the attraction in the $i_q - \omega$ plane only when $i_d = \frac{v_d}{R}$. The sections $i_d = \frac{v_d}{R} + 0.001$ and $i_d = \frac{v_d}{R} - 0.001$ were also verified for the same duration. Then we repeat the exercise for the planes $i_q - i_d$ and $i_d - \omega$, respectively when $\omega = 0$ and $i_q = 0$. For these nine sections, there is no intersection between chaos region and the saddle equilibrium, as stated in the paper.

Now we can observe the dynamics around the symmetric equilibria. We consider another section of the space in order to view the two symmetric equilibria. The plane of these two equilibria is $i_d = -\frac{n^2 {k_t}^2 + Rb}{n^2 k_t L}$.

The two equilibria belong to their respective region of basin of attraction as illustrated in Fig. 7. The region in green represents the initial conditions for which the hidden chaotic set is visualized. For the stable region in blue (red) color, the trajectories converge to $S_1(S_2)$. At $v_d = -28.6$V, these two symmetric equilibria are stable.

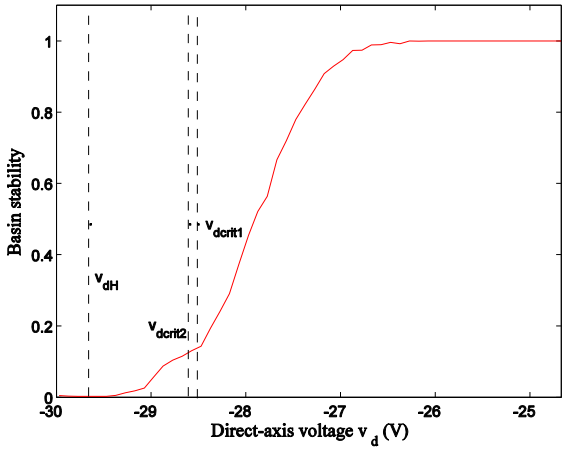

(a) Basin stability for I_{s_1} region

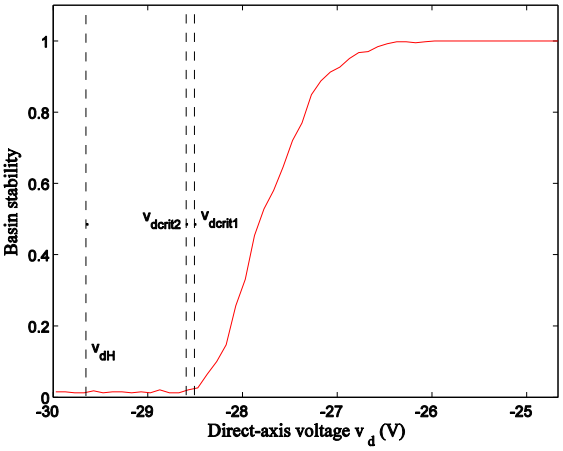

(b) Basin stability for I_{s_2} region

Fig. 4. Basin stability of BLDCM.

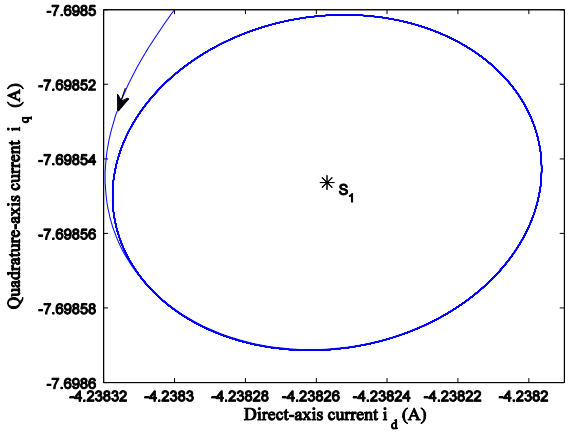

(a) Limit cycle 1 with initial conditions at $-7.6985, -4.2383, -58.9271$ ^{T}

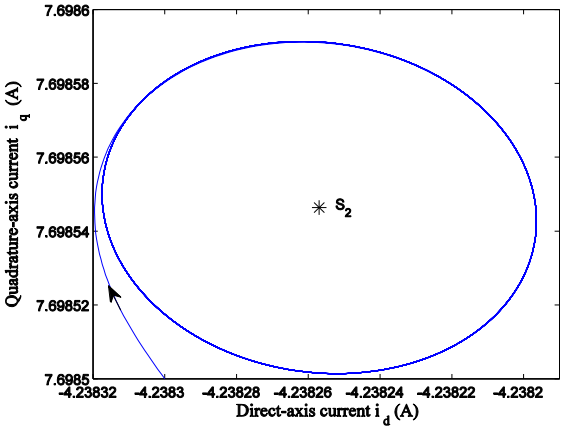

(b) Limit cycle 2 with initial conditions at $7.6985, -4.2383, 58.9271$ ^{T}

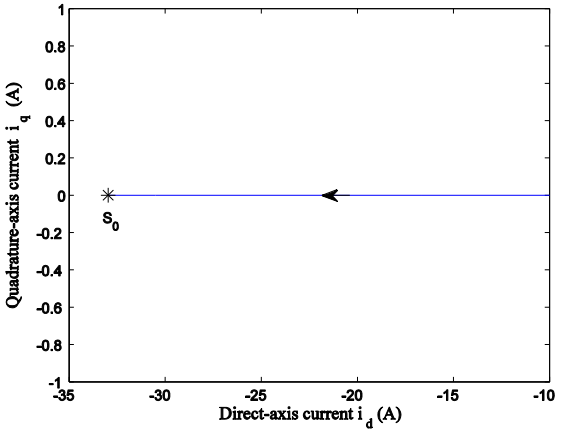

(c) Stability with initial conditions at $0, -10, 0$ ^{T}

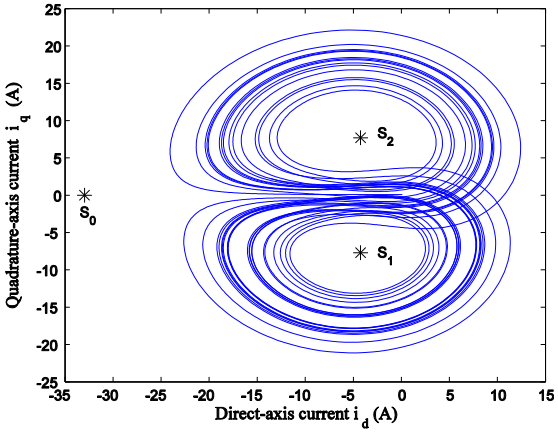

(d) Chaos with initial conditions at $0.1, 0.1, 0.1$ ^{T}

Fig. 5. Coexistence of different dynamic modes.

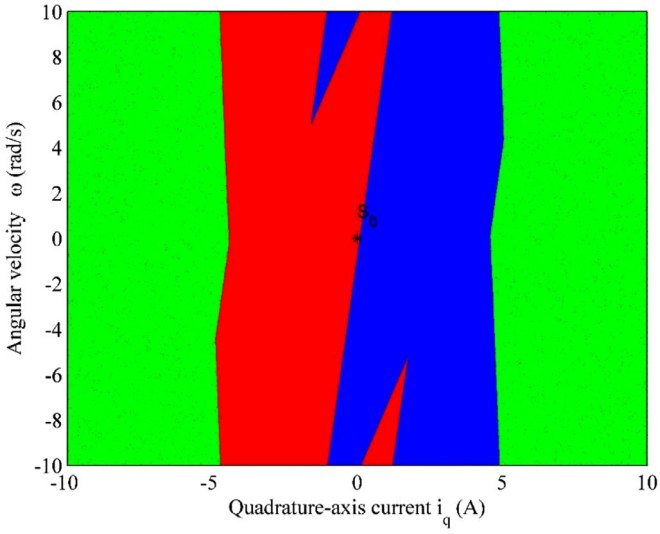

Fig. 6. Different regions of basin of attraction around the saddle equilibrium S_0. (For interpretation of the references to color in the text, the reader is referred to the web version of this article.).

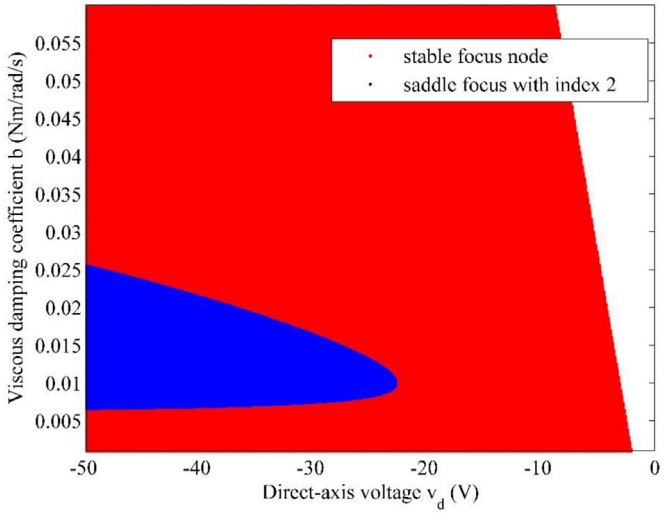

Fig. 8. Distribution of eigenvalues of symmetric equilibria. (For interpretation of the references to color in the text, the reader is referred to the web version of this article.).

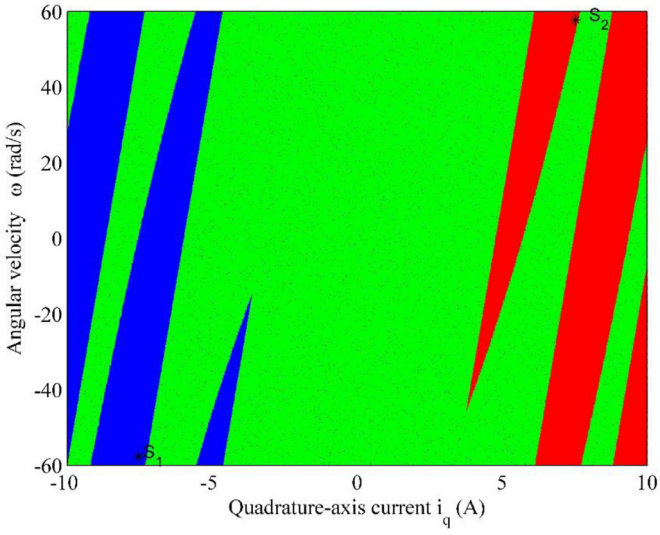

Fig. 7. Different regions of basin of attraction around the stable focus equilibria S_1 and S_2. (For interpretation of the references to color in the text, the reader is referred to the web version of this article.).

The distribution of eigenvalues that show the type of stability of these two equilibria is illustrated in Fig. 8. The red region represents the parameter space where the two equilibria are stable focus nodes. And the blue region represents the space where the two equilibria are saddle focus nodes with index 2. Hidden chaotic set exists only in the region (red) of stable focus node in Fig. 8.

There have been several attempts to localize such hidden chaotic set. Firstly, we applied the method of perpetual points (PP) [32–33]. By using the perpetual points to identify the hidden chaotic attractor we found that six perpetual points, excluding the fixed points. But with the parameters of hidden chaos, these perpetual points turned out to be complex in the region of interest. The perpetual points can be obtained by finding the higher derivative of the dynamical system, actually by extending the dimension of the system. Maybe by extending to higher orders (more than second order), the PP could be found for BLDCM. We stopped at the second order to avoid more complexity. Apart from the PP, we have utilized the method of homotopy [36]. In this method we look at the different stable and unstable manifolds of the saddle equilibrium and we note the behavior of transition. By considering Fig. 3 we show the appearance and disappearance of hidden chaos. In green the initial conditions are taken as $[i_q(0), i_d(0), \omega(0)]^{\mathrm{T}} = [2, 2, \ 2]^{\mathrm{T}}$ and the blue and red trajectories have initial conditions on the unstable manifold of the saddle origin equilibrium with $v_d = -28.626565874764298$V, these three trajectories are chaotic and combine as illustrated in Fig. 3(e). But when $v_d = -28.626565874764296$V, the green trajectory is chaotically hidden while the blue and red trajectories converge around the equilibria as shown in Fig. 3(d).

Therefore, there exists some transition around $v_d = -28.626565874764297$V. This transition value cannot be detected by bifurcation diagram. On the other hand, around the value $v_d = -28.53$V hidden chaos ceases to exist. With the method of homotopy, $v_{dcrit2} = -28.626565874764297$V and $v_{dcrit1} = -28.53$V are identified. In all the experiment setups we consider that the system runs until $t = 300$s. For longer time frame, the chaotic set demonstrates its transient features. In the next section we briefly describe the transient features of hidden chaotic set of BLDCM.

4.3. Transient properties

The effect of transient properties of hidden chaotic set of the BLDCM is observed in Fig. 9(a)-(b).

After some time $t > 418$s, the hidden chaotic set originating from $[i_q(0), i_d(0), \omega(0)]^{\mathrm{T}} = [2, 2, \ 2]^{\mathrm{T}}$ converges to the equilibria S_2 as illustrated in Fig. 9(b). The fixed step-size is 0.000001 and the ODE method is ODE5 (Dormant-Prince). While this duration seems shorter than with Singh *et al.* [30] where $t < 570$s the fixed step-size is smaller.

It is also well known that the transient chaos can be converted into permanent chaos with techniques of chaos maintenance or preservation [44], especially for chaos requiring applications such as mixing or compacting and grinding. Rather than focusing only on asymptotic states of the BLDCM, transient dynamics are relevant in terms of observation, prediction and even control. It is beyond the scope of this paper to apply techniques to maintain chaos.

Nevertheless, we can find the initial conditions with longer transient time. We apply the concept of critical surfaces [34–35] to find initial conditions of longer transient time. The critical surfaces are related to the concept of regular points and perpetual points.

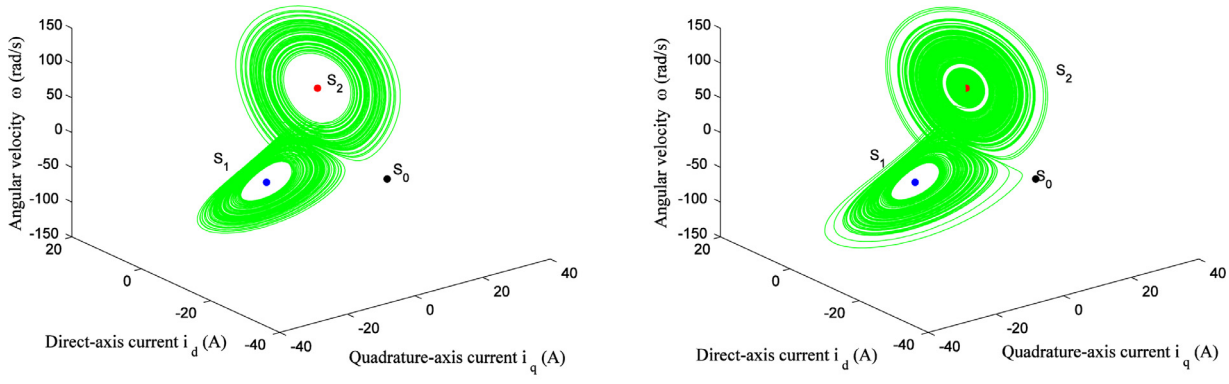

Fig. 9. Transient hidden chaos.

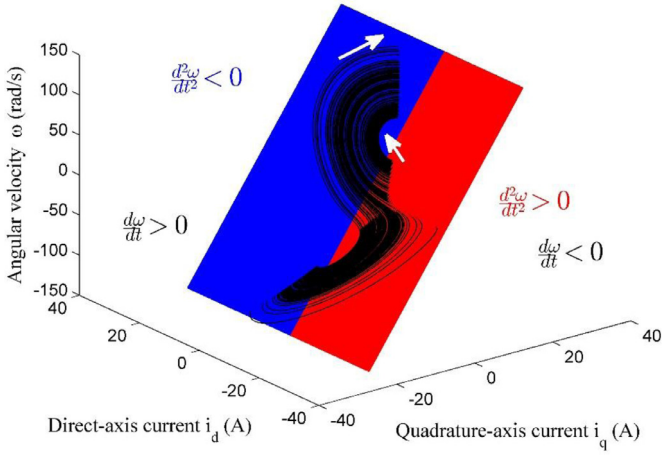

Fig. 10. Dynamics of BLDCM chaotic attractor around critical surfaces.

We find the points in each state where acceleration is zero while velocity is non-zero in order to reach the final state in maximum time. It should be reminded that perpetual points are related to regular points [34] and critical surfaces [35]. The x_i critical velocity surface is the surface at which the velocity of the ith variable equal zero, i.e., $\dot{x}_i = 0$ (for each $i = 1, 2....N$, N being the number total of states). The x_i critical acceleration surface is the surface at which the acceleration of the ith variable equal zero, i.e., $\ddot{x}_i = 0$ (for each $i = 1, 2....N$, N being the number total of states).

For the BLDCM, we consider the angular velocity as the state of observation. The critical velocity surface $\dot{\omega} = 0$ is the plane that crosses the chaotic set and the critical acceleration surface is $\ddot{\omega} = 0$.

From Fig. 10, the critical acceleration surface is the intersection between the red part of the plane $\ddot{\omega} > 0$ and the blue part of the plane $\ddot{\omega} < 0$. The attractor enters the plane on the blue region (as shown with the arrow) and returns on the red region as shown by the arrow.

The plane separates two regions of space: $\dot{\omega} > 0$ and $\dot{\omega} < 0$. We locate around the intersection of the two regions in Fig. 10 with the initial conditions $i_q(0) = -45.0168619$, $i_d(0) = -11.770379$, $\omega(0) = -74.080004$. We find a much longer transient time 1025s, with the step-size 0.000001. In the case the attempt has been to find the initial conditions such that the time for convergence is the longest possible.

Equally, we utilize optimization techniques such as the Broyden-Fletcher-Goldfarb-Shanno (BFGS) algorithm for finding iteratively optimal solutions for unconstrained nonlinear objective

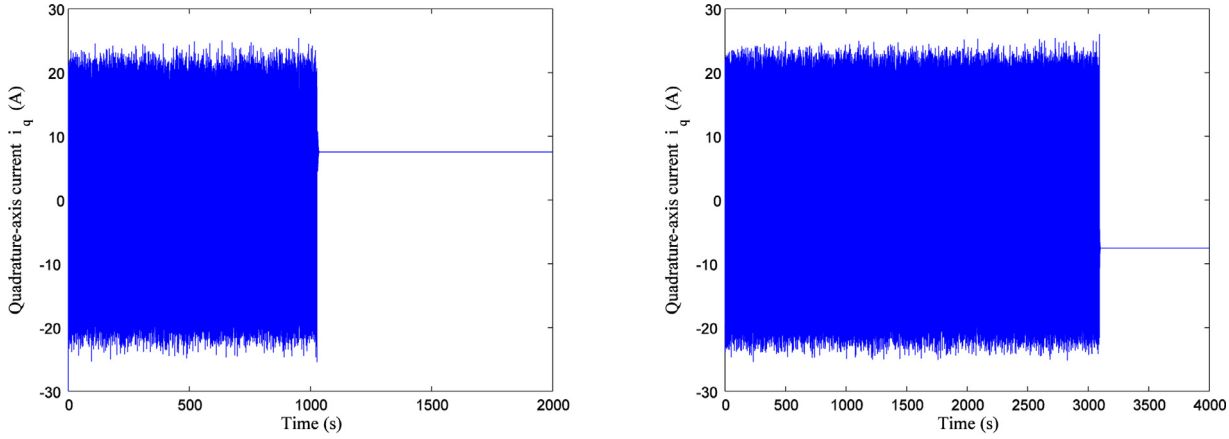

Fig. 11. Transient chaos in time series.

functions [37]. The objective function is optimized by two tests. Either it is maximized or its inverse is minimized. In this way we avoid to fall on the equilibrium as the equilibrium will make the objective function become zero. The objective function is defined as

$$F(i_q, i_d, \omega) = \left(\frac{di_q}{dt}\right)^2 + \left(\frac{di_d}{dt}\right)^2 + \left(\frac{d\omega}{dt}\right)^2, \tag{8.1}$$

or

$$F(i_q, i_d, \omega) = -\left[\left(\frac{di_q}{dt}\right)^2 + \left(\frac{di_d}{dt}\right)^2 + \left(\frac{d\omega}{dt}\right)^2\right]. \tag{8.2}$$

From $[1, -2, 4]^{\mathrm{T}}$ by using the BFGS method, the following initial conditions were obtained as points of minimum velocity $i_q(0) = 15.408297155754024$, $i_d(0) = -4.238256932654184$, $\omega(0) = 117.9400523033024$.

The duration of transient dynamics has improved with the method of the critical velocity and acceleration surfaces by a factor of 2.452 as in Fig. 11(a). Also, transient time has improved with the optimization technique like BFGS by a factor of 7.416as illustrated in Fig. 11(b). Thus, depending on initial conditions, the transient time of the hidden chaotic set can vary.

5. Conclusion

In this paper the dynamical properties of the BLDCM, a type of permanent magnet synchronous motor (PMSM), were explored. The model of the BDLCM was reviewed and linked to another model of PMSM. Comments on the number of equilibria and their stability of the PMSM were made. The homoclinic bifurcation of the BLDCM as an important transition phase towards chaos was observed and analyzed. Broadly, transition of the BLDCM towards chaos was studied. This transition was studied locally with different bifurcations such as pitchfork, Hopf bifurcations and globally with homoclinic bifurcation, manifolds and invariant sets. From the number of equilibria, the concept of multistability was examined in terms of basin stability that is related to basin of attraction. Some cases of multistability were illustrated. Hidden chaos in BLDCM was highlighted from the definition based on the basin of attraction of the saddle equilibrium. The BLDCM demonstrates hidden chaotic set and the equilibria that generate hidden chaos are clearly identified as stable focus nodes. The localization of hidden chaos was achieved through the method of homotopy. Finally, the transient properties of hidden chaos were explained. Two methods (critical surfaces and BFGS) were used to demonstrate the dependence of transient time on initial conditions. In this paper, comments were made on a recent paper, which reported hidden chaos in PMSM. Since the number of equilibria is actually different, chaos is not hidden but self-excited. In the future, hidden chaos should be investigated with regard to basin of attractions in 3D. In addition, the interactions of different parameters in the generation of hidden and self-excited chaos should be further investigated.

Declaration of Competing Interest

The authors declare that they have no known competing financial interests or personal relationships that could have appeared to influence the work reported in this paper.

CRediT authorship contribution statement

Philippe Faradja: Conceptualization, Writing - original draft, Data curation, Formal analysis, Writing - review & editing, Validation. **Guoyuan Qi:** Data curation, Writing - review & editing, Validation.

Acknowledgments

This work is supported by the National Natural Science Foundation of China (61873186) and the Natural Science Foundation of Tianjin City (17JCZDJC38300).

Reference

[1] Lorenz EN. Deterministic nonperiodic flow. J Atmos Sci 1963;20(2):130–48.
[2] Rössler OE. An equation for continuous chaos. Phys Lett A 1976;57(5):397–8.
[3] Chen G, Ueta T. Yet another chaotic attractor. Int J Bifurc Chaos 1999;9(07):14651.
[4] Qi G, Chen G, Du S, Chen Z, Yuan Z. Analysis of a new chaotic system. Phys A 2005;352:295–308.
[5] Qi G, Chen G, van Wyk MA, van Wyk BJ, Zhang Y. A four-wing chaotic attractor generated from a new 3D quadratic autonomous system. Chaos Solitons Fractals 2008;38:705–21.
[6] Rössler OE. An equation for hyperchaos. Phys Lett A 1979;71:155–7.
[7] Qi G, van Wyk MA, van Wyk BJ, Chen G. On a new hyperchaotic system. Phys Lett A 2008;372:124–36.
[8] Miillin T. Chaos in physical systems. In: Crilly AJ, Earnshow RA, Jones H, editors. Fractals and chaos. New York: Springer; 1991. p. 237–45.
[9] Shinbrot T, Grebogi C, Wisdom J, Yorke JA. Chaos in a double pendulum. Am J Phys 1992;60(6):491–9.
[10] Zhu Q, Ishitobi M. Experimental study of chaos in a driven triple pendulum. J Sound Vib 1999;227(1):230–8.
[11] Kitio Kwuimy CA, Woafo P. Dynamics, chaos and synchronization of self-sustained electromechanical systems with clamped-free flexible arm. Nonlinear Dyn 2008;53:201–13.
[12] Montava Belda MA. A route to chaos in electromechanical systems: phase space attraction basin switching. Int J Bifurc 2009;19(7):2363–75.
[13] Hemati N. Strange attractors in brushless DC motors. IEEE Trans Circuits Syst I 1994;41(1):40–5.
[14] Chau KT, Wang Z. Chaos in electric drive systems: analysis, control and application. Singapore: John Wiley & Sons Pte Ltd; 2011.
[15] Xia C. Permanent magnet brushless DC motor drives and controls. Singapore: John Wiley &Sons Pte.Ltd; 2012.
[16] Kuznetsov NV, Kuznetsov OA, Leonov GA, Vagaytsev VI. Hidden attractor in Chua's circuits. In: Proceedings of ICINCO; 2011. p. 279–83.
[17] Leonov GA, Kuznetsov NV, Vagaitsev VI. Localization of hidden Chua's attractors. Phys Lett A 2011;375(23):2230–3.
[18] Leonov G, Kuznetsov N, Vagaitsev V. Hidden attractor in smooth Chua systems. Phys D 2014;241(18):1482–6.
[19] Kuznetsov NV, Leonov GA, Mokaev TN, Seledzhi SM. Hidden attractor in the Rabinovich system, Chua circuits and PLL. In: AIP Conference Proceedings, 1738; 2016.
[20] Leonov GA, Kuznetsov NV, Mokaev TN. Homoclinic orbits, and self-excited and hidden attractors in a Lorenz-like system describing convective fluid motion. Eur Phys J Spec Top 2015;224:1421–58.
[21] Munmuangsaen B, Srisuchinwong B. A hidden chaotic attractor in the classical Lorenz system. Chaos Solitons Fractals 2018;107:61–6.
[22] Yuan Q, Yang FY, Wang L. A note on hidden transient chaos in the Lorenz system. Int J Nonlinear Sci Numer Simul 2017;18:427–34.
[23] Wei Z, Moroz I, Sprott JC, Akgul A, Zhang W. Hidden hyperchaos and electronic circuit application in a 5D self-exciting homopolar disc dynamo. Chaos 2017;27:033101.
[24] Jafari S, Sprott JC, Nazarimehr F. Recent new examples of hidden attractors. Eur Phys J Spec Top 2015;224:1469–76.
[25] Kiseleva MA, Kuznetsov NV, Leonov GA, Neittaanmäki P. Hidden oscillations in drilling system actuated by induction motor. IFAC Proc 2013;46:86–9.
[26] Kuznetsov NV. Hidden attractors in fundamental problems and engineering models: a short survey. In: Duy VH, Dao TT, Zelinka I, Choi HS, Chadli M, editors. AETA 2015: recent advances in electrical engineering and related sciences, lecture notes in electrical engineering, 371. Cham: Springer International Publishing; 2016. p. 13–25.
[27] Pham VT, Volos C, Jafari S, Kapitaniak T. Coexistence of hidden chaotic attractors in a novel no-equilibrium system. Nonlinear Dyn 2016;87(3):2001–10.
[28] Li C, Sprott JC. Variable-boostable chaotic flows. Optik 2016;127(22):10389–98.
[29] Pham VT, Akgul A, Volos C, Jafari S, Kapitaniak T. Dynamics and circuit realization of a no-equilibrium chaotic system with a boostable variable. AEU 2017;78:134–40.
[30] Singh JP, Roy BK, Kuznetsov NV. Multistability and hidden attractors in the dynamics of permanent magnet synchronous motor. Int J Bifurc Chaos 2019;29(4):1950056.
[31] Faradja P, Qi G. Energy bifurcation and energy patterns of the BLDCM systems manifolds in the hidden chaos mode. In: Proceedings of 11th IWCFTA, 8; 2018.
[32] Prasad A. Existence of perpetual points in nonlinear dynamical systems and its applications. Int J Bifurc Chaos 2015;25(02):1530005.
[33] Dudkowski D, Prasad A, Kapitaniak T. Perpetual points and hidden attractors in dynamical systems. Phys Lett A 2015;379(40–41):2591–6.
[34] Dudkowski D, Prasad A, Kapitaniak T. Describing chaotic attractors: regular and perpetual points. Chaos 2018;28:033604–1–10.
[35] Godara P, Dudkowski D, Prasad A, Kapitaniak T. New topological tool for multistable dynamical systems. Chaos 2018;28(11):111101–6.

[36] Dudkowski D, Jafari S, Kapitaniak T, Kuznetsov NV, Leonov GA, Prasad A. Hidden attractors in dynamical systems. Phys Rep 2016;637:1–50.
[37] Rao SS. Engineering optimization: theory and practice. 4th ed. New Jersey: Wiley Eastern Ltd; 2009.
[38] Li Z, Park JB, Joo YH, Zhang B, Chen G. Bifurcations and chaos in a permanent-magnet synchronous motor. IEEE Trans Circuits Syst I 2002;49:383–7.
[39] Faradja P, Qi G. Local bifurcation analysis of brushless DC motor. Int Trans Electr Energy Syst 2019;29(2):e2710.
[40] Shilnikov LP. On a new type of bifurcation of multidimensional dynamical systems. Sov Math Dokl 1969;10:1368–71.
[41] Li Z, Chen G, Halang WA. Homoclinic and heteroclinic orbits in a modified Lorenz system. Inf Sci 2004;165:235–45.
[42] Menck PJ, Heitzig J, Marwan N, Kurths J. How basin stability complements the linear-stability paradigm. Nat Phys 2013;9:89–92.
[43] Kuznetsov NV, Mokaev TN. Numerical analysis of dynamical systems: unstable periodic orbits, hidden transient chaotic sets, hidden attractors, and finite-time Lyapunov dimension. J Phys Conf Ser 2019;1205(1):012034.
[44] Lai YC, Tél T. Transient chaos: complex dynamics on finite time scales. Applied mathematical sciences. New York: Springer-Verlag; 2011.